ARMY RESEARCH LABORATORY

Energy Partitioning and Microstructural Observations Related to Perforation of Titanium and Steel Targets

by N. L. Rupert, F. I. Grace, W. Huang,
L. E. Murr, and C-S. Niou

ARL-TR-1453 August 1997

The findings in this report are not to be construed as an official Department of the Army position unless so designated by other authorized documents.

Citation of manufacturer's or trade names does not constitute an official endorsement or approval of the use thereof.

Destroy this report when it is no longer needed. Do not return it to the originator.

Army Research Laboratory
Aberdeen Proving Ground, MD 21005-5066

ARL-TR-1453 **August 1997**

Energy Partitioning and Microstructural Observations Related to Perforation of Titanium and Steel Targets

N. L. Rupert, F. I. Grace
Weapons and Materials Research Directorate, ARL

W. Huang, L. E. Murr, C-S. Niou
The University of Texas at El Paso

Abstract

This report presents an analysis of two target materials and the associated energetics related to the initial penetration into the target and perforation as the penetrator exits the target. Impact tests were conducted for tungsten alloy rods striking rolled homogeneous armor (RHA) and titanium alloy plates. Rod impact velocities were nominal 1,500 and 2,000 m/s. Target thicknesses were chosen so that the rods would overmatch the targets and lose some 200 m/s during penetration. The tests utilized flash x-rays to determine rod residual lengths and velocities, and target plug features, to include thicknesses and velocities. From these observables, experimental determination of the corresponding kinetic energies (KEs) and estimates for the fracture energies were obtained. Also, in each case, target material adjacent to penetration channel walls was examined by optical and electron microscopy and x-ray diffraction to gain further insight into deformation processes (cavity expansion) during penetration. The analytic penetration model gave results that were in good agreement with the experimental observables. In addition, it was observed that the RHA follows traditional plastic flow of cavity expansion while titanium alloy shows deformation features that deviate significantly. The report discusses possible causes for these differences.

Table of Contents

INTENTIONALLY LEFT BLANK.

List of Figures

List of Tables

INTENTIONALLY LEFT BLANK.

1. Introduction

Recent advances in theoretical penetration mechanics by Grace [1] allow the problem of kinetic energy (KE) rod impact with plates at impact velocities extending to hypervelocity to be separated into two phases. These phases include (1) an initial penetration into the target and (2) a following perforation of the target as the rod exits the target rear surface. The model used in this study provided a framework through which the overall energetics could be analyzed theoretically as demonstrated by Rupert and Grace [2]. Previous analytic approaches to the problem have included adaptations of the Tate analysis for semi-infinite targets by Zook [3], the semi-empirical formulas of Lambert [4], and applications of "hydrocodes" [1, 3, 5], for example. Collectively, these approaches have produced a large body of knowledge about penetration and perforation that allows engineering estimates of target efficiencies against long rods. However, certain aspects of the penetration process have not been adequately addressed. These aspects include the nature of target deformation in terms of changes in microstructure of the material, where and how the KE of the rod is dissipated in the target, and details of target material failure and fracture during perforation.

A recently developed model for penetration/perforation of single plates [1] is used to track details of the penetration events at impact velocities extending to the hydrodynamic regime, wherein the process is considered to take place in two separate phases. These phases include (1) an initial penetration into the plate target and (2) a following perforation of the target as the rod exits the target rear surface. Since the analysis provides mass-velocity relationships and estimates for the fracture energies, it is used here to analyze the energetics of penetration and perforation processes. The present work also includes experimental test results for tungsten alloy (WA) long rods that were fired at high velocity against two targets of practical interest (i.e., rolled homogeneous armor [RHA] and titanium-6% aluminum-4% vanadium alloy [Ti-6/4]). Optical and transmission electron microscopy examinations were conducted on the target materials after perforation. X-ray diffraction was conducted to determine any structural phase shifts in the Ti-6/4 material. This report includes results that demonstrate significant differences in the impact response of RHA and Ti-6/4 in terms of the

dissipation of energy in these targets and presents supporting calculations and experimental observations.

2. Experimental Approaches and Results

2.1 Rod-Impact Tests. Rod-impact tests were designed so that the penetration efficiencies of RHA and Ti-6/4 plate targets could be compared. The penetrators were fired from a laboratory gun consisting of a Bofors' 40-mm gun breech assembly with a custom-made 40-mm smoothbore barrel that was positioned approximately 3 m in front of the targets. High-speed (flash) radiography was used to record and measure projectile pitch, yaw, striking velocity, residual rod length, residual rod velocity, and plug thickness and velocity. Two pairs of orthogonal x-ray tubes were positioned in the vertical and horizonal planes along the shot line in front of the target (as illustrated in Figure 1). An additional pair of x-ray tubes was positioned in the horizonal plane along the shot line behind the target. Propellant weight was adjusted for desired nominal velocities (v_s) of 1,500 m/s and 2,000-m/s. Shots that had a total yaw in excess of 2° were considered "no tests," and those data were disregarded.

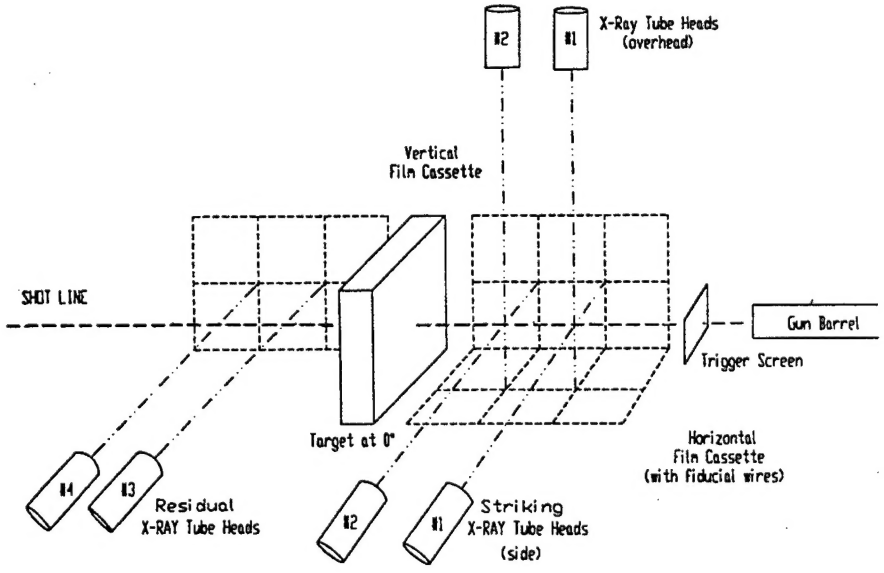

Figure 1. Experimental Setup.

The rod projectile used in the impact experiments had a mass of 65 g, a length (ℓ_0) of 78.2 mm, a diameter of 7.82 mm, and a hemispherical nose shape. The rods were composed of WA, to include tungsten (93%), nickel (4.91%), and iron (2.11%), and were manufactured by Teledyne Firth Sterling. The rods were fabricated using the nominal X-21 process with 25% swaging. Nominal material properties are as follows: density - 17.7 g/cm^3, hardness - Rockwell C Scale 40.5–42.6, yield strength - 1.089–1.169 GPa, ultimate strength - 1.131–1.213 GPa, and elongation - 5.8–10.6 % [6, 7].

Targets included RHA (MIL-A-12560, Class 3 Steel) and titanium alloy, Ti-6/4 (6% aluminum and 4% vanadium). Two slightly different plate thicknesses were used for the RHA targets: 44.69 mm with an areal density of 350.8 kg/m^2 and a nominal 40 mm with a corresponding areal density of 307.3 kg/m^2. The Ti-6/4 target thickness was 70.21 mm, having an areal density of 312.4 kg/m^2.

Table 1 presents results of the impact experiments that were measured from the radiographs. It is to be noted that for both RHA and Ti-6/4 targets, higher rod-impact velocity resulted in greater rod residual length and velocity. The trend is not nearly so pronounced for residual rod length, but nonetheless, is consistent with expectations based on similar results by Zook and Frank [8] and Stilp [9]. The analysis of Grace [1] suggests that residual rod length is a slowly varying function of impact velocity, especially at relatively high velocities (over 1,500 m/s), when the rod overmatches the target substantially, as is the case here. On the other hand, residual rod velocity is expected to continue to increase at least linearly with impact velocity [1, 2, 3, 8], even at high velocity, and the present results show that trend.

Target channel profiles were measured from recovered targets after the shot and are given in Table 2. Figure 2 provides a schematic showing measurement locations relative to the target cross section. Two diameter measurements were recorded for each location to capture any possible noncircular shape of the channel. Mostly, there are only small differences in the gross channel features between the target materials beyond the presence of a spall ring at the Ti-6/4 target exit hole.

Only slight differences in entrance-hole diameters, resulting from cratering, and penetration-channel diameters were observed. Exit-hole diameters and spall-ring diameters appear to depend on

Table 1. Ballistic Results

Target	Pitch (°)	Yaw (°)	Striking Velocity (m/s)	Residual Rod Length (mm)	Residual Rod Velocity (m/s)
44.69-mm RHA	−0.25	0.75	1,507	39.7	1,297
	−0.50	0.00	1,510	38.6	1,297
40.03-mm RHA	0.00	0.00	1,973	41.7	1,893
39.91-mm RHA	−0.75	0.00	1,997	41.4	—[a]
70.21-mm Ti-6/4	−0.50	0.25	1,501	26.1	1,110
	−1.25	0.25	1,501	26.5	1,118
	0.00	0.75	1,959	31.0	1,770
	1.50	0.00	1,980	31.0	1,831

[a] Lost second x-ray flash.

Table 2. Hole Measurements

Target	Entrance-Hole Diameter (mm)		Penetration-Channel Diameter (mm)		Exit-Hole Diameter (mm)	
	Min.	Max.	Min.	Max.	Min.	Max.
44.69-mm RHA	19	20	15	15	23	27
	18	20	13	14	27	29
40.03-mm RHA	—[b]	—[b]	17	17	23/38[a]	23/38[a]
39.91-mm RHA	—[b]	—[b]	18	21	28/37[a]	28/37[a]
70.21-mm Ti-6/4	20	27	15	16	18/44[a]	22/46[a]
	18	22	13	15	18/43[a]	20/46[a]
	—[b]	—[b]	14	15	25/49[a]	25/54[a]
	—[b]	—[b]	17	19	23/46[a]	24/54[a]

[a] For measurements denoted xx/yy, yy is the spall ring diameter.

[b] Obscured by Pusher Plate Impact.

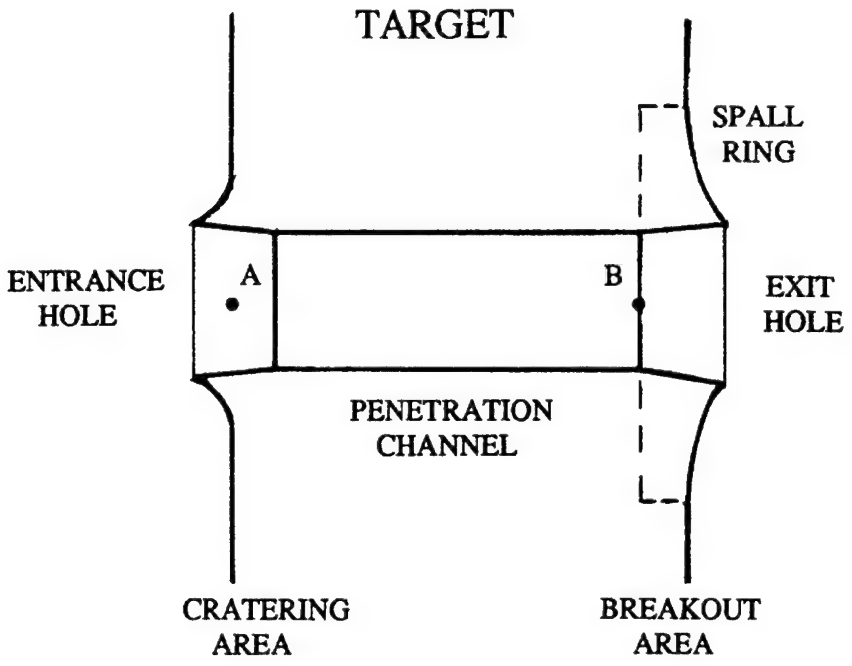

Figure 2. Target Cross Section Schematic, Where A Is the Original Surface, and B Is The Point Where Erosion Stops and Breakout Starts.

target material. Ti-6/4 exit-hole diameters averaged 20 mm and 24 mm in diameter for 1,500 m/s and 2,000 m/s, respectively, compared to the slightly larger 26.5-mm diameter averaged of the RHA steel plates. Penetration-channel diameter for the RHA demonstrated a slight increase with increased penetrator striking velocity. Ti-6/4's penetration channel may have increased with increased penetrator striking velocity, but the measurements are not conclusive. Plug thicknesses were obtained from flash x-ray coverage from behind the targets at 1,500 m/s. The average plug thickness was estimated to be 13 mm for the Ti-6/4 and 4 mm for the RHA. Plugs could not be separated from spall on the x-rays from the 2,000-m/s tests.

2.2 Microstructural and X-ray Diffraction Investigations. Both optical microscopy and transmission electron microscopy were used to study deformation of material near the channel wall. The midsection region of each target specimen was polished and etched for optical metallography.

For RHA, the etchant consisted of 2.5% nitol (2.5% nitric acid [HNO_3], 97.0% methanol [CH_3OH], and water [H_2O]) using etching times of roughly 35 s. The etchant for the Ti-6/4 target material consisted of 0.2-liter water, 5-ml hydrogen fluoride (HF), and 10-ml nitric acid, using etching times of approximately 17 s.

Specimens for transmission electron microscopy (TEM) were systematically extracted very close to the channel wall by using a stop-off lacquer on the channel surface and electropolishing from the rear. In addition, samples were sliced from representative sections at varying distances along the channel midsection, extending to distances of more than 20 mm from the channel surface. These slices were ground and polished to a thickness of about 100 μm, and 3-mm-diameter disks were punched from the slices. A Tenupol-3 electropolishing system was used to produce electron transparent thin sections utilizing the following etchants: for the RHA steel samples, 1.2 liters of methanol were mixed with 0.2 liters of perchloric acid ($HClO_4$), and electropolishing was performed at −15° C; for Ti-6/4 alloy, 1.4 liters of methanol and 0.14 liters of hydrochloric acid (HCl) were employed at −15° C. TEM analysis was done in a Hitachi H-8000 analytical TEM operated at 200-kV accelerating potential in the conventional TEM (CTEM) mode.

Figure 3(a) shows the longitudinal section of the RHA penetration channel. The corresponding optical (metallographic) views and TEM views of typical microstructures very near the channel surface are shown in Figure 3(b) and (d). Corresponding views at distances far removed from the channel are presented in Figure 3(c) and (e). There is extensive plastic deformation extending from the channel wall (shown in Figure 3[b]) that consists of gross grain elongation with very fine, elongated dislocation cell structures intermixed with carbides (shown in Figure 3[d]). Figure 3(e) illustrates the fact that the undisturbed RHA microstructure is a complex intermixing of ferrite grains, carbides, and a heavy dislocation structure. The average Vickers microhardness in that region is 0.32 GPa (using a 1-kgf load), while, in contrast, that taken at a distance of about 1 mm from the channel surface is about 0.4 GPa. Previously reported hardness profiles [10] taken outward from the channel surface indicate that the increased hardness and, therefore, the plastic zone due to the penetration process, extends radially to a distance of 70% of the channel radius or about 9.3 mm into the material beyond the channel surface.

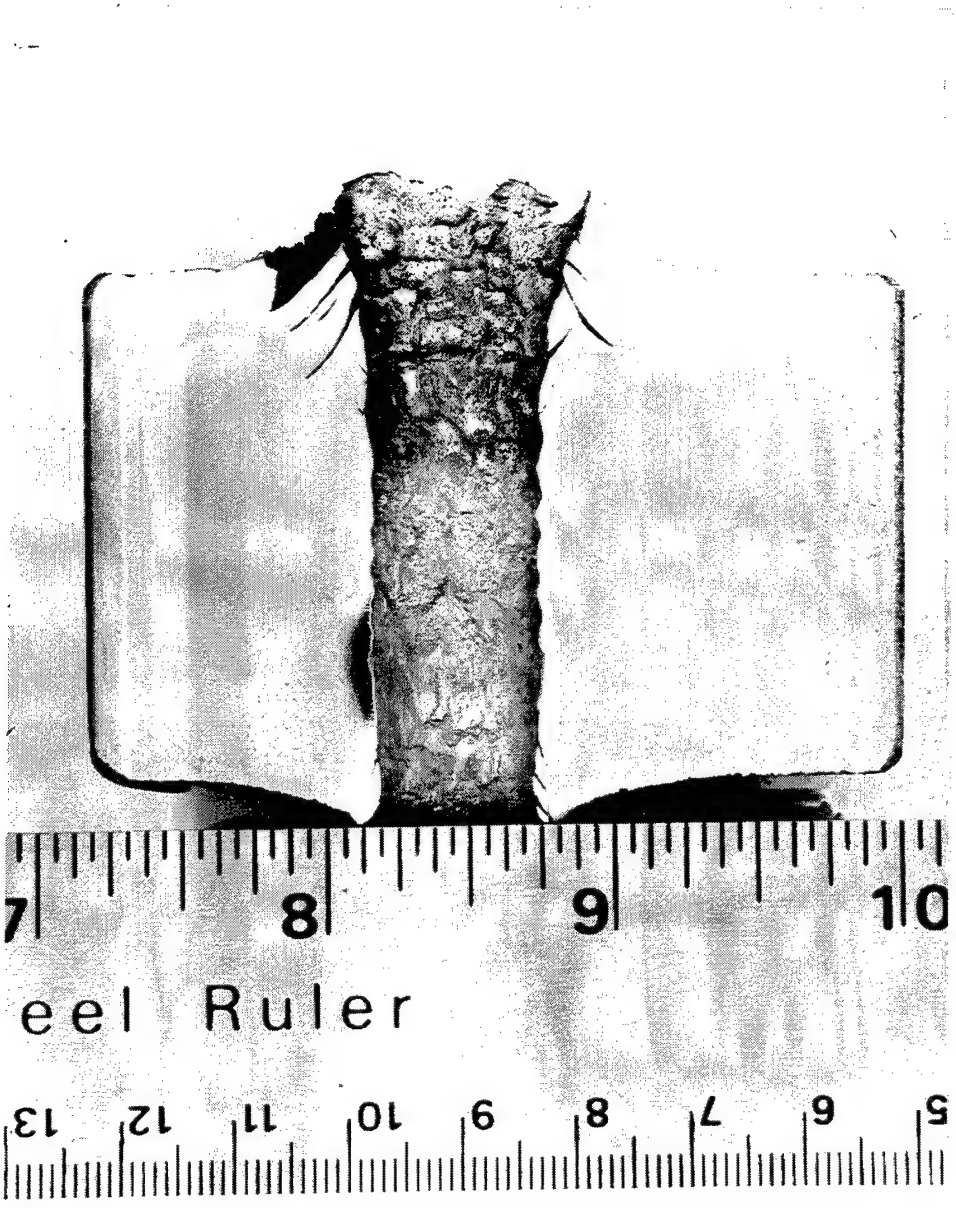

Figure 3. RHA Penetration-Channel-Related Microstructures. (a) RHA Penetration-Channel Half-Section Reference.

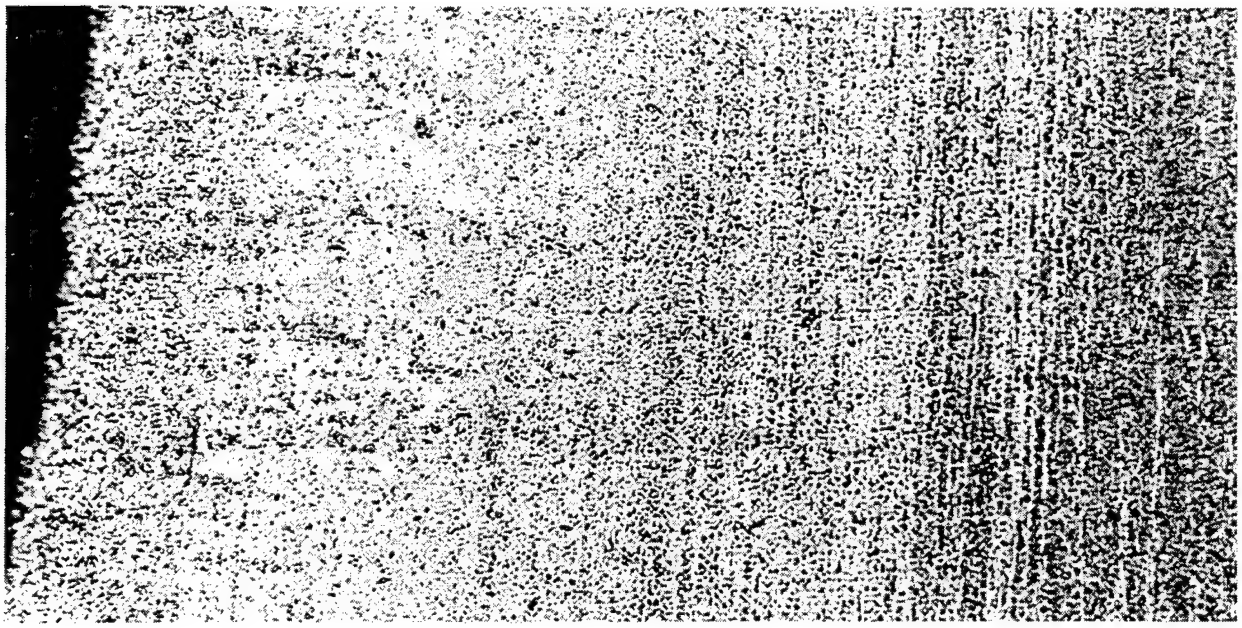

(b)

(c)

Figure 3. RHA Penetration-Channel-Related Microstructures (continued). (b) Light Microscope View of Microstructure Extending From the Penetration-Channel Surface at the Midsection. (c) Light Microscope View of the RHA Target Microstructure 20 mm From the Penetration-Channel Surface.

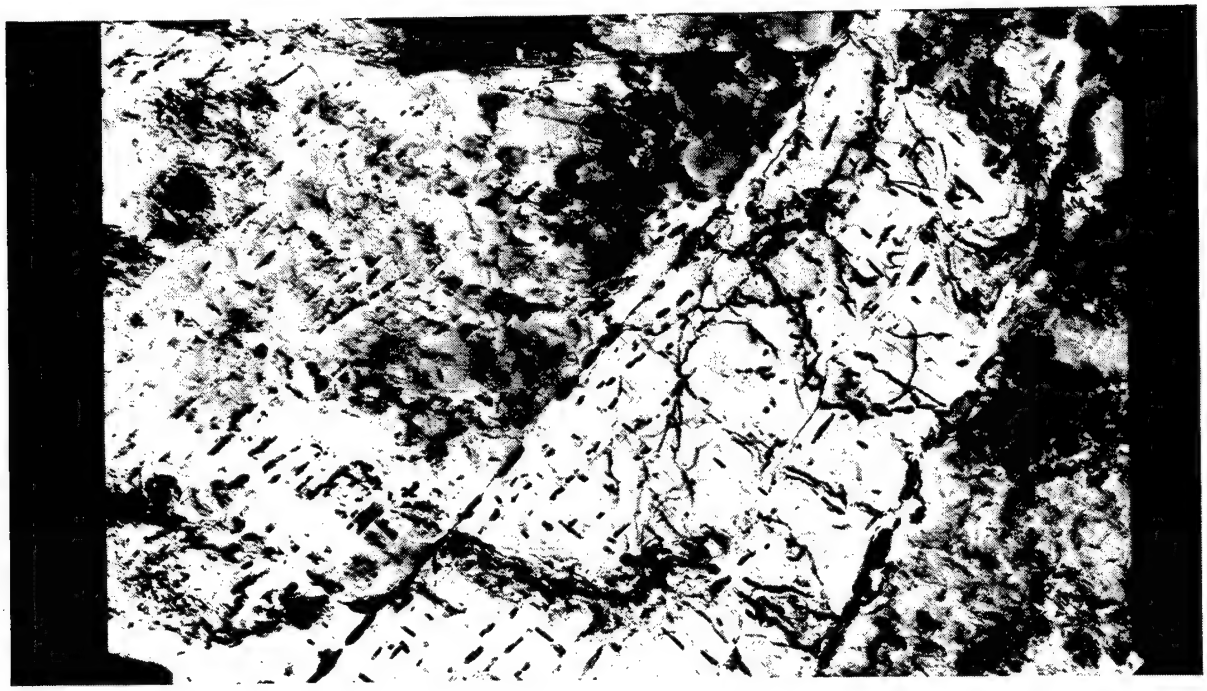

(d)

(e)

Figure 3. RHA Penetration-Channel-Related Microstructures (continued). (d) TEM Bright-Field Image of RHA Penetration-Channel-Related Microstructure Roughly 0.2 mm From the Penetration-Channel Surface. (e) TEM Bright-Field Image of the Initial RHA Target Microstructure Corresponding to (c).

Figure 4(a) shows the Ti-6/4 penetration-channel half section. TEM and optical microstructures close to the channel surface are shown in Figure 4(b) and (d), respectively. Their undisturbed counterparts at a distance far from the channel surface are shown in Figure 4(c) and (e). For Ti-6/4, no discernable differences in grain structure are seen in the optical microscopy at locations near to or far removed from the channel surface. This result is in stark contrast to that for RHA and suggests that no gross plastic deformation (grain elongation) exists in the Ti-6/4 material adjacent to the channel surface. However, TEM observations only 0.1 mm from the channel surface reveal (contrast Figure 4[c] and [e]) heavy dislocation structures within the 2-phase, α/β (hexagonal-close-packed [hcp]/body-centered-cubic [bcc]) regimes. It should be noted that grain elongation requires considerably more expended energy in deformation than does the generation of dislocations within the grains. The Ti-6/4 has a hardness profile [10] that shows an increase in hardness starting at the channel surface and continuing outward to about 40% of the channel radius or about 4 mm beyond the channel surface. There were no observations of shear bands associated with the channel midsection as shown for the Ti-6/4 target in Figure 4(b) and (d). Shear bands were also not prominent near the midsection of penetration channel in RHA as well.

Additional differences between the two target materials occur in the formation of the plugs and spall rings. The RHA exhibits signs of a higher degree of ductile failure in the form of material flow and tearing. In contrast, the Ti-6/4 target does not exhibit these gross features, but does resemble a more brittle failure. The conspicuous lack of plastic flow and tearing in Ti-6/4 was previously observed by Woodward, Baxter, and Scarlett [11] and Holt et al. [12] for plug formation at lower impact velocities. Further, the appearance of a spall ring in Ti-6/4 at 1,500-m/s impact velocity (and not in RHA) together with the previously mentioned observations suggest that Ti-6/4 is more susceptible to brittle failure under impact conditions than RHA.

As a check on any possible shifts in the α/β structure of the Ti-6/4 material during penetration, x-ray diffraction (Cu-Kα) spectra were also compared between the initial material (far removed from the channel surface) and that within 1 mm of the channel surface. Results showed the β (bcc) phase to dominate, and there was no change in the material near the channel surface. All peak intensities

Figure 4. Ti-6/4 Penetration-Channel-Related Microstructures. (a) Ti-6/4 Penetration-Channel Half-Section Reference.

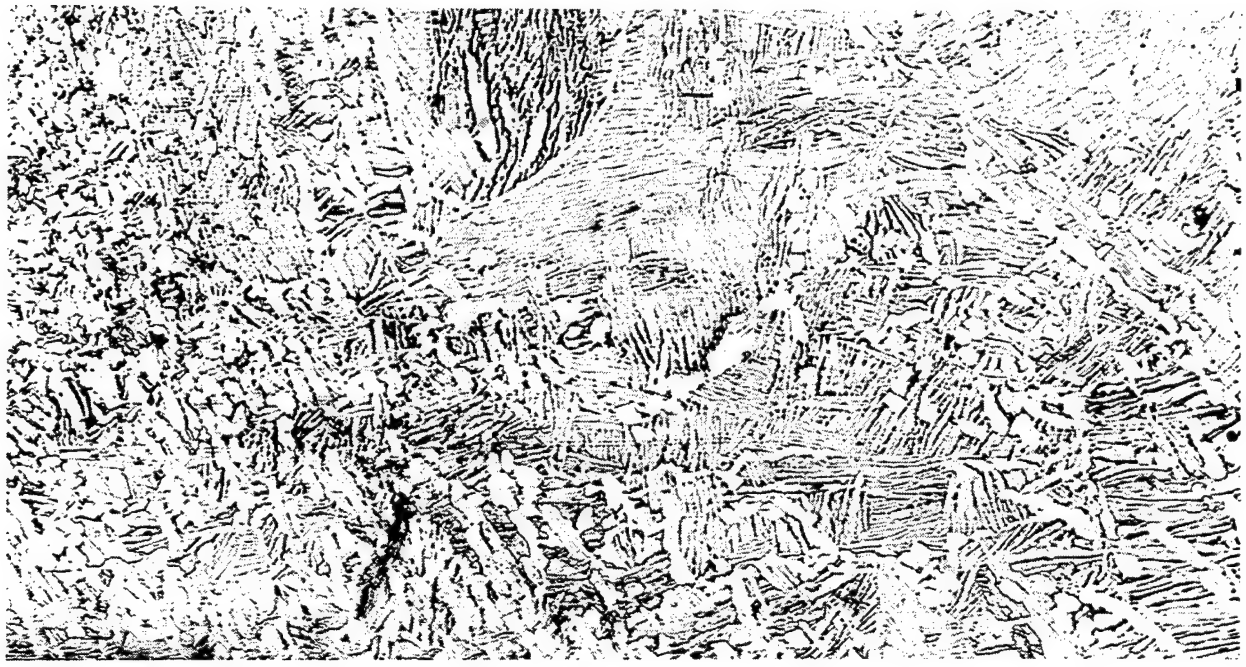

(b)

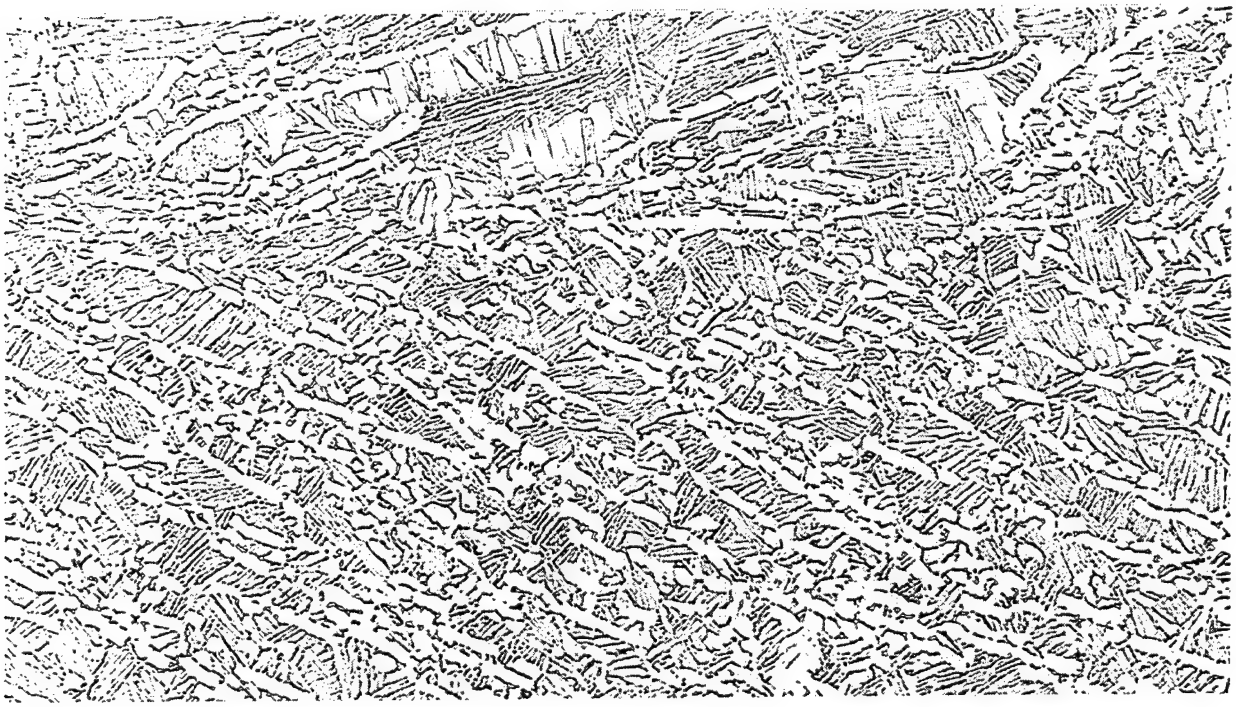

(c)

Figure 4. Ti-6/4 Penetration-Channel-Related Microstructures (continued). (b) Light Microscope View of Microstructure Extending From the Penetration-Channel Surface at the Midsection. (c) Light Microscope View of the Ti-6/4 Target Microstructure 20 mm From the Penetration-Channel Surface.

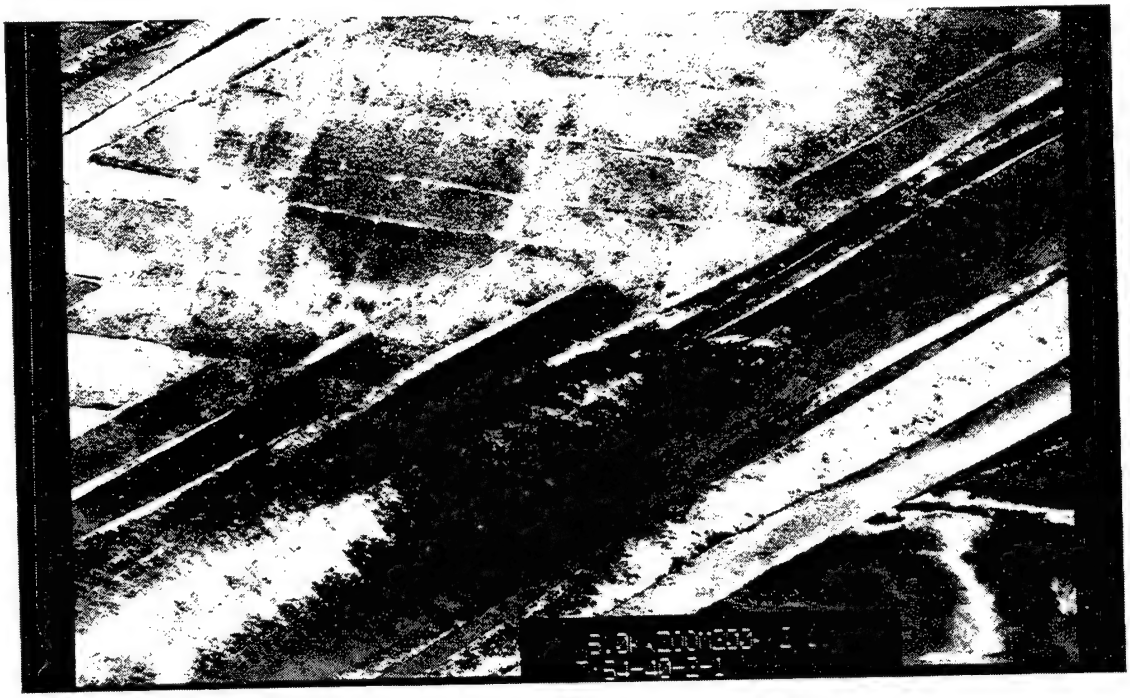

(d)

(e)

Figure 4. Ti-6/4 Penetration-Channel-Related Microstructures (continued). (d) TEM Bright-Field Image of Ti-6/4 Penetration-Channel-Related Microstructure Roughly 0.2 mm From the Penetration-Channel Surface. (e) TEM Bright-Field Image of the Initial Ti-6/4 Target Microstructure Corresponding to (c).

were enhanced uniformly for the material near the channel surface, which is consistent with the typical deformation-related dislocation density increases shown previously.

Since no gross plastic deformation was observed in Ti-6/4, nor an indication of a change in the distribution of phases within the Ti-6/4, it would appear that the penetration process must involve some other mechanism. Furthermore, since the Ti-6/4 has a tendency for brittle failure under impact as was discussed previously, it is plausible that the penetration involves extensive fracturing of the material. In Figure 3(a), a small chip can be seen clinging to the channel surface. Since the cavity has reasonable axial symmetry elsewhere along its length, it is of interest that no such material particle is present on the opposite side of the channel surface. The cracks about and within the chip suggest that the cavity may have been formed by excavation of fractured material.

3. Energy Analysis

Calculations of energy partitioning during sequential phases of penetration and perforation follow the analysis of Grace [1]. In this model, the penetration phase involves a simultaneous process of rod deceleration and erosion (reduction in its length) and target acceleration and erosion or plastic flow (reduction in its thickness). As such, the dynamics indicate that the rod length is not entirely consumed during penetration, nor is the target thickness. Thus, the analysis provides the unconsumed target thickness z_c, when target consumption (penetration) stops as

$$z_c = z_0 \exp\left[-\frac{\rho_t}{2S_t} u_0^2\right], \tag{1}$$

where z_0 is the target initial thickness, ρ_t is the target density, S_t is the target strength, and u_0 is the penetration rate. Grace [1] also provides a near-linear relationship between u_0 and striking velocity v_s. The consumed target thickness (penetration into the target) $P_c = z_0 - z_c$ corresponds to the distance between point A and point B in Figure 1. Also, the analysis provides residual rod length ℓ_r, based on its initial length ℓ_0, and rod velocity v_e at point B and the acceleration of localized target material in front of the penetrator to a velocity u_0 as well. In general, the velocity of the remaining

rod at the end of the penetration phase will be greater than that of the target material (i.e. $v_e > u_0$). This condition promotes breakout. With masses and velocities defined by the momentum interactions contained within the theory, it is possible to calculate the associated KEs at the end of the penetration phase as inputs to the perforation phase, given an estimate for the cross-sectional area of the localized target material [2].

For the perforation phase, Grace [1] treats the subsequent rod-target interaction problem as inelastic so that after perforation, the residual rod and target plug velocities are equal. The energy balance under these circumstances is

$$(M_r + M_c)v_r^2 = M_r v_e^2 + M_c u_0^2 - 2E_f , \tag{2}$$

where E_f is the energy required to fracture the remaining target material of thickness z_c, M_r is the residual rod mass, M_c is the residual target mass (assuming its area), and v_r is the residual rod velocity. Thus, KEs of the major masses are accounted for in the analysis. It is not necessary to account for the KE of the spall ring since the x-rays indicate that spall-ring velocity did not exceed one-tenth of the residual rod velocity even though its mass may be on the order of the plug mass.

The fracture model for the plug is essentially that of Woodward and Crouch [13] and Holt et al. [12], who determined the work required for plug separation (shear) from the surrounding target plate. In terms of Grace's notation, the fracture energy becomes

$$E_f = \frac{1}{2}\pi d_s S_s z_c^2 , \tag{3}$$

where S_s is the shear strength of the target material (taken here as $S_s = S_t/\sqrt{3}$, where S_t is a nominal strength for the target material), and d_s is the plug diameter. The energy required to fracture the spall ring is neglected for the cases of interest here. From the experiments it was noted that at lower velocities, the depth of the spall ring (as measured on the exit surface of the target) was about 5 mm for the Ti-6/4 while the plug thickness was 13 mm. Since fracture energy as given by equation (3) depends on the thickness squared, that for the spall ring is small (15%) relative to the fracture energy

of the plug. There was no observed spall ring on the RHA target impacted at 1,500 m/s. At high velocity, the fracture energy due to both plugging and spall-ring formation is relatively small compared to the high KEs of the rod and target masses. This notion follows from equations (1) and (3) since z_c gets exceedingly small as rod striking velocity and, therefore, penetration rate u_0 is increased.

Using the previous analysis, calculations were carried out for each of the rod-target combinations through a range of velocities that encompass the experimental conditions. The analysis used the average of all measured penetration-channel exit-hole diameters as the plug diameter. These diameters were 21 mm for RHA and 18 mm for Ti-6/4. Also, the following material properties were used: for RHA, $\rho_t = 7.85$ g/cm^3, $S_t = 1.09$ GPa, $S_s = 0.629$ GPa, and $C_0 = 5{,}170$ m/s; for Ti-6/4, $\rho_t = 4.45$ g/cm^3, $S_t = 1.14$ GPa, $S_s = 0.658$ GPa, and $C_0 = 6{,}070$ m/s. Properties for the tungsten alloy rods were taken to be $\rho_p = 17.3$ g/cm^3 and $S_p = 1.51$ GPa, where S_p is the penetrator strength. Table 3 contains calculated results corresponding to the experimental impact conditions.

Table 3. Calculated Values

Target	Striking Velocity (m/s)	Residual Rod Length (mm)	Residual Rod Velocity (m/s)	Plug Mass (g)
44.69-mm RHA	1,507	39.91	1,271	12.508
	1,510	38.96	1,275	12.360
40.03-mm RHA	1,973	48.64	1,904	1.252
39.91-mm RHA	1,997	48.92	1,931	1.095
70.21-mm Ti-6/4	1,501	27.93	1,096	20.758
	1,959	34.23	1,769	5.243
	1,980	34.52	1,797	4.871

Figure 5 presents a comparison of the calculations and experimental data for the residual rod length and velocity and plug thickness. Since the analytic results agreed well with the experimental results, they provided a valid basis for the energy analysis. The results of the energy calculations to include the KEs are presented in Table 4. The quantities of interest include initial rod KE before

impact, its KE after erosion and deceleration at the end of penetration into the target (first phase), the KE of accelerated target mass at the end of the first phase, the KE of the residual rod and target mass (plug) after perforation (second phase), and the fracture energy required to separate the plug from the target surrounds (fracture energy of breakout). The amount of KE dissipated during rod erosion is that lost by the rod during penetration (first phase) and is based on the difference between its initial KE before impact and that at the end of the penetration phase.

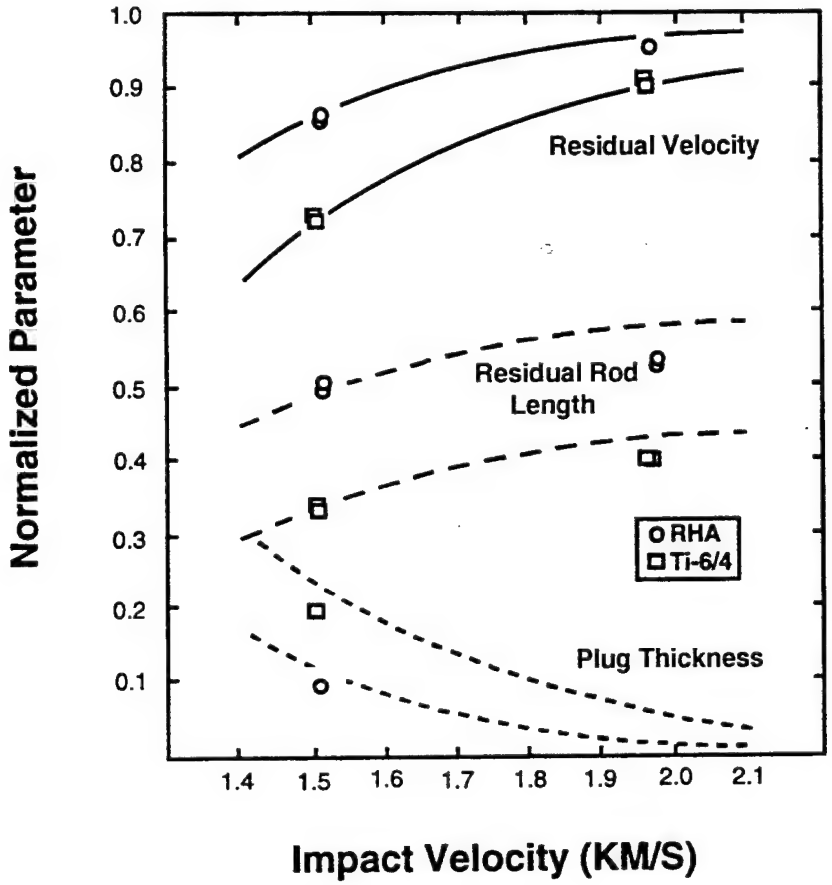

Figure 5. Comparison of Theoretical Calculations (Curves) and Experimental Data for RHA and Ti-6/4 to Include Residual Rod Velocity (v_r/v_s), Residual Rod Length (ℓ_r/ℓ_0), and Plug Thickness (z_c/z_0).

The amount of KE dissipated from the rod by erosion and deceleration during penetration can appear in several forms to include KE of erosion products, work required to create the channel

Table 4. Energy Partition

Target	Striking Velocity (m/s)	Initial Rod KE (J)	KE Dissipated During Rod Erosion (J)	Plug KE Before Breakout (J)	Fracture Energy at Breakout (J)	Residual Rod KE (J)	Plug KE After Breakout (J)
44.69-mm RHA	1,507 1,510	75,206 75,506	41,629 42,543	6,271 6,141	177 172	27,129 26,650	10,102 10,046
40.03-mm RHA	1,973	128,909	53,224	1,487	2	74,196	2,269
39.91-mm RHA	1,997	132,064	53,951	1,357	1	76,755	2,041
70.21-mm Ti-6/4	1,501 1,951 1,980	74,609 126,050 129,826	53,475 76,434 78,542	4,863 4,406 4,206	2,154 137 119	14,117 45,073 46,905	12,467 8,204 7,865

cavity, acceleration of the target mass (plug), and heat. Table 4 indicates that the rod loses more KE to these factors when penetrating Ti-6/4 than it does in RHA plates. This result stems from the penetration path being longer in the Ti-6/4 while the target strengths (resistance to penetration) are similar. Also, since the plug thickness according to equation (1) depends on initial plate thickness, and the energy for plug fracture is greater by equation (3), considerably more plug fracture energy is expended in the Ti-6/4 target. Consequently, these two considerations provide a rationale for the greater efficiency of Ti-6/4 against these rods.

Table 5 provides the results of energy rate calculations and displaced target mass estimates. Time rates are based on the calculated time [1] between the initial contact of the penetrator at point A (Figure 2) and the time the penetrator stops eroding at point B (Figure 2). Length rates are based on length of rod eroded for the penetrator, the distance between the point of impact (point A, Figure 2), and the onset of breakout (point B, Figure 2) for the target. Mass rates are based on the mass eroded from the penetrator and the displaced target mass in the penetration channel (target).

When the amount of KE lost by the rod per unit path length in the target is considered, as shown in Table 5, the two target materials appear to be equivalent. Thus, the total energy expended is consistent with the work done on the target, which is proportional to the integrated effects of target

Table 5. Energy Rates and Displaced Mass

Target	Striking Velocity (m/s)	KE Dissipated Time (J/μs)	KE Dissipated Length (J/mm)		KE Dissipated Mass (J/g)		Displaced Target Mass in Penetration Channel (g)
			Penetrator	Target	Penetrator	Target	
44.69-mm RHA	1,507 1,510	671 689	1,073 1,071	1,037 1,058	1,275 1,272	1,182 1,205	35.2 35.3
40.03-mm RHA	1,973	1,456	1,771	1,345	2,104	1,534	34.7
39.91-mm RHA	1,997	1,506	1,812	1,365	2,153	1,559	34.6
70.21-mm Ti-6/4	1,501 1,959 1,980	586 1,194 1,247	1,053 1,718 1,778	1,001 1,159 1,185	1,252 2,042 2,112	810 938 959	66.0 81.5 81.9

resistance times displacement. The displacement (path length) is greater for Ti-6/4. On the other hand, since it takes more time to penetrate the Ti-6/4 target, KE losses during penetration per unit time are similar for the two target materials.

Table 5 also shows that the penetrator mass and length based KE rates for Ti-6/4 are similar to that for RHA. Thus, the mechanism for creating cavities in Ti-6/4 must involve a process that is similar in energy requirements as plastic deformation in RHA. However, the microstructural observations validate that the Ti-6/4 did not exhibit extensive plastic deformation. Further, the present efforts have also shown no significant change in the α/β phase distribution; thus, this factor cannot contribute to energy absorption. Since Ti-6/4 is more susceptible to brittle fracture, it is possible that fracturing of the material initially located within the channel may occur during penetration. If this material could separate itself from the channel surface, possibly by shear, then this hypothesis is consistent with all of the observations and analyses conducted in this study. Thus, there is reason to pursue an energy-consuming mechanism during the creation of the channel in Ti-6/4 that involves extensive fracturing of Ti-6/4 material and its excavation during the penetration process.

4. Summary of Results

The problem of target penetration and perforation has been addressed using multiple approaches to include (1) an energy analysis of the penetration and perforation processes, (2) specifically designed long rod-impact tests using tungsten alloy rods at 1,500 and 2,000 m/s against RHA and Ti-6/4 plates of equal areal density, and (3) metallurgical investigations of material adjacent to penetration channels created by impact. The experimental work and the analysis showed that Ti-6/4 is a substantially more mass-efficient target material than RHA. The dynamics contained within the analysis showed that the increased efficiency of the Ti-6/4 was due to higher energy dissipation by the rod in that target material. While the Ti-6/4 target strength was similar to RHA, penetration paths (amount of target thickness) and, therefore, the forces times displacements were considerably larger for Ti-6/4 plates of equal areal density. Plug thicknesses were larger for the Ti-6/4, so the additional energy required for plug separation also contributed.

The experiments and associated calculations indicated that length-based KE dissipation rates were similar in the formation of the penetration channels in both Ti-6/4 and RHA. However, the metallurgical observations of the channel walls showed a decisive difference in the process by which penetration takes place. The grain elongation and deformation structures observed show that RHA follows the classical cavity expansion related to plastic flow about the rod during penetration. On the other hand, the Ti-6/4 did not exhibit these gross plastic deformation features. Thus, since the Ti-6/4 has known tendencies for brittle failure, and since some evidence of brittle failure was observed within the penetration channel, it is plausible that Ti-6/4 undergoes extensive fracturing with possible excavation of the fractured material during penetration. Such a process would not require large amounts of plastic flow, but rather much more energy expended in fracture, and this view is consistent with the collective experimental observations and analyses conducted in this investigation.

5. References

1. Grace, F. I. "Long-Rod Penetration into Targets of Finite Thickness at Normal Impact." *Int. J. Impact Engng.*, vol. 16, pp. 419–433, 1995.

2. Rupert, N. L., and F. I. Grace. "Impact Studies of Rod Projectiles Against Titanium and Steel Targets." *Proc. Int. Conf. on Materials (EXPLOMET '95)*, pp. 257–264, 1995.

3. Zook, J. A. Private communication. March 1993.

4. Lambert, J. P. "A Residual Velocity Predictive Model for Long Rod Penetrators." ARBRL-MR-02828, U.S. Army Ballistic Research Laboratory, Aberdeen Proving Ground, MD, April 1978.

5. Grace, F. I., T. Sherrick, and K. D. Kimsey. "Penetration Studies of Rods Impacting Targets of Finite Thickness Using the CTH Eulerian Hydrocode." *Military, Government, and Aerospace Simulation, Simulation Series (SCS)*, vol. 27, pp. 53–58, 1995.

6. Teledyne Firth Sterling. Material certification sheet, BRL contract no. DAAD05-90-C-0431, LaVergne, TN, 1991.

7. Farrand, T. G. Unpublished data. U.S. Army Ballistic Research Laboratory, Aberdeen Proving Ground, MD, 1991.

8. Zook, J. A., and K. Frank. "Comparative Penetration Performance of Tungsten Alloy 1/d = 10 Long Rods with Different Nose Shapes Fired at Rolled Homogeneous Armor." BRL-MR-3480, U.S. Army Ballistic Research Laboratory, Aberdeen Proving Ground, MD, 1985.

9. Stilp, A. J. Private communication. June 1993.

10. Huang, W., L. E. Murr, C-S. Niou, N. L. Rupert, and F. I. Grace. "Metallurgical Studies of Deformation and Failure Patterns from Targets Impacted by Long-Rod Penetrators." *Proc. Int. Conf. on Materials (EXPLOMET '95)*, El Paso, TX, pp. 265–272, 1995.

11. Woodward, R. L., B. J. Baxter, and N. V. Y. Scarlett. "Mechanisms of Adiabatic Shear Plugging Failure in High Strength Aluminum and Titanium Alloys." *Inst. Phys. Conf. Ser. No. 70*, 3rd Conf. Mech. Prop. High Rates of Strain, Oxford, England, pp. 525–532, 1984.

12. Holt, W. H., W. Mock, Jr., W. G. Soper, C. S. Coffrey, V. Ramachandran, and R. W. Armstrong. "Reverse-Ballistic Impact Study on Shear Plug Formation and Displacement in Ti6A14V Alloy." *J. Appl. Phys.*, vol. 73, pp. 3753–3759, 1993.

13. Woodward, R. L., and I. G. Crouch. "A Computational Model of the Perforation of Multi-Layer Metallic Laminates." MRL-RR-9-89, DSTO Materials Research Laboratory, Maribyrnong, Victoria, Australia, 1989.

NO. OF COPIES	ORGANIZATION
2	DEFENSE TECHNICAL INFORMATION CENTER DTIC DDA 8725 JOHN J KINGMAN RD STE 0944 FT BELVOIR VA 22060-6218
1	HQDA DAMO FDQ DENNIS SCHMIDT 400 ARMY PENTAGON WASHINGTON DC 20310-0460
1	CECOM SP & TRRSTRL COMMCTN DIV AMSEL RD ST MC M H SOICHER FT MONMOUTH NJ 07703-5203
1	PRIN DPTY FOR TCHNLGY HQ US ARMY MATCOM AMCDCG T M FISETTE 5001 EISENHOWER AVE ALEXANDRIA VA 22333-0001
1	PRIN DPTY FOR ACQUSTN HQS US ARMY MATCOM AMCDCG A D ADAMS 5001 EISENHOWER AVE ALEXANDRIA VA 22333-0001
1	DPTY CG FOR RDE HQS US ARMY MATCOM AMCRD BG BEAUCHAMP 5001 EISENHOWER AVE ALEXANDRIA VA 22333-0001
1	DPTY ASSIST SCY FOR R&T SARD TT T KILLION THE PENTAGON WASHINGTON DC 20310-0103
1	OSD OUSD(A&T)/ODDDR&E(R) J LUPO THE PENTAGON WASHINGTON DC 20301-7100

NO. OF COPIES	ORGANIZATION
1	INST FOR ADVNCD TCHNLGY THE UNIV OF TEXAS AT AUSTIN PO BOX 202797 AUSTIN TX 78720-2797
1	DUSD SPACE 1E765 J G MCNEFF 3900 DEFENSE PENTAGON WASHINGTON DC 20301-3900
1	USAASA MOAS AI W PARRON 9325 GUNSTON RD STE N319 FT BELVOIR VA 22060-5582
1	CECOM PM GPS COL S YOUNG FT MONMOUTH NJ 07703
1	GPS JOINT PROG OFC DIR COL J CLAY 2435 VELA WAY STE 1613 LOS ANGELES AFB CA 90245-5500
1	ELECTRONIC SYS DIV DIR CECOM RDEC J NIEMELA FT MONMOUTH NJ 07703
3	DARPA L STOTTS J PENNELLA B KASPAR 3701 N FAIRFAX DR ARLINGTON VA 22203-1714
1	SPCL ASST TO WING CMNDR 50SW/CCX CAPT P H BERNSTEIN 300 O'MALLEY AVE STE 20 FALCON AFB CO 80912-3020
1	USAF SMC/CED DMA/JPO M ISON 2435 VELA WAY STE 1613 LOS ANGELES AFB CA 90245-5500

NO. OF
COPIES ORGANIZATION

1 US MILITARY ACADEMY
MATH SCI CTR OF EXCELLENCE
DEPT OF MATHEMATICAL SCI
MDN A MAJ DON ENGEN
THAYER HALL
WEST POINT NY 10996-1786

1 DIRECTOR
US ARMY RESEARCH LAB
AMSRL CS AL TP
2800 POWDER MILL RD
ADELPHI MD 20783-1145

1 DIRECTOR
US ARMY RESEARCH LAB
AMSRL CS AL TA
2800 POWDER MILL RD
ADELPHI MD 20783-1145

3 DIRECTOR
US ARMY RESEARCH LAB
AMSRL CI LL
2800 POWDER MILL RD
ADELPHI MD 20783-1145

ABERDEEN PROVING GROUND

2 DIR USARL
AMSRL CI LP (305)

NO. OF COPIES	ORGANIZATION
1	HQDA SARD TT J APPEL WASHINGTON DC 20310-0103
3	DIR DARPA LTC R KOCHER (3 CPS) 3701 N FAIRFAX DR ARLINGTON VA 22203-1714
3	CDR US ARMY RSCH OFC K LYER K IYER J BAILEY PO BOX 12211 4033 MIAMI BLVD RESEARCH TRIANGLE PARK NC 27709
2	CDR US ARMY MRDEC AMSMI RD ST WF D LOVELACE M SCHEXNAYER REDSTONE ARSENAL AL 34898-5250
3	CDR US ARMY TACOM RD&E CENTER AMCPM ABMS SA J ROWE AMSTA RSS J THOMPSON AMSTA RSK S GOODMAN WARREN MI 48397-5000
1	CDR USA BLVR RD&E CTR STRBE NAN TECH LIBRARY FT BELVOIR VA 22060-5166
6	CDR US ARMY ARDEC SMCAR AAE W J PEARSON TECH LIBRARY PICATINNY ARSENAL NJ 07806-5000
1	PM TANK MAIN ARMNT SYSTEMS SSAE AR TMA MT PICATINNY ARSENAL NJ 07806-5000

NO. OF COPIES	ORGANIZATION
1	PM SURVIVABILITY SYS SFAE ASM SS T T DEAN WARREN MI 48397-5000
1	CDR NGIC W MARLEY 220 SEVENTH AVE CHARLOTTESVILLE VA 22901-5391
1	CDR ERO USARDSG (UK) R REICHENBACH PSC 802 BOX 15 FPO AE 09499-1500
1	USMC MCRDAC PM GRNDS WPNS BR D HAYWOOD FIREPOWER DIV QUANTICO VA 22134
1	CH OF NAVAL RSCH OFC OF NAVAL TECH A J FAULSTICH ONT 23 BALLSTON TOWERS ARLINGTON VA 22217
1	NAVAL WPNS CTR TECH LIBRARY CHINA LAKE CA 93555
4	CDR NSWC R GARRETT R 12 J FOLTZ R 32 H DEJARNETTE R 32 TECH LIBRARY 10901 NEW HAMPSHIRE AVE SILVER SPRING MD 20903-5000
1	NUSC NEWPORT S DICKINSON CODE 8214 NEWPORT RI 02841
1	NSWC DAHLGREN DIV G 22 ROWE DAHLGREN VA 22448

NO. OF COPIES	ORGANIZATION
1	NAVAL POST GRAD SCHOOL J STERNBERG CODE EW MONTEREY CA 93943
2	MSD ENL W DYESS J FOSTER EGLIN AFB FL 32542-5000
1	BOMBS & WARHEAD BRANCH W COOK MUNITIONS DIVISION EGLIN AFB FL 32542
1	AIR FORCE ARMNT LAB TECH LIBRARY EGLIN AFB FL 32542
10	DIR SANDIA NATIONAL LABS M KIPP DIV 1533 R GRAHAM DIV 1551 P YARRINGTON D GRADY MS 0821 D CRAWFORD ORG 1533 M FORRESTAL LUK J ASAY MS 0548 R BRANNON MS 0820 M KIPP MS 0820 TECH LIBRARY PO BOX 5800 ALBUQUERQUE NM 87185
1	DEFENSE NUCLEAR AGENCY TECH LIBRARY 6801 TELEGRAPH RD ALEXANDRIA VA 22192
1	AMERICAN EMBASSY BONN DR R ROBINSON UNIT 21701 BOX 165 APO AE 09080
1	CIA OSWR DSD W WALTMAN ROOM 5P0110 NHB WASHINGTON DC 20505

NO. OF COPIES	ORGANIZATION
10	DIR LOS ALAMOS NATIONAL LAB G E CORT F663 R KARPP MS 1960 F ADDESSIO F GAC M BURKETT B HOGAN W GASKILL J CHAPYAK MS G787 S MARSH MS 970 M 6 TECH LIBRARY PO BOX 1663 LOS ALAMOS NM 87545
11	DIR LLNL J E REAUGH L 290 M FINGER MS 35 D BAUM D STEINBERG J REAUGH L32 M WILKINS M J MURPHY R GOGOLEWSKI MS L290 R LANDINGHAM L369 R WHIRLEY L122 TECH LIBRARY PO BOX 808 LIVERMORE CA 94550
1	NEW MEXICO TECH D EMARY TERA GROUP SOCORRO NM 87801
1	JET PROPULSION LAB M ADAMS IMPACT PHYSICS GROUP 4800 OAK GROVE DR PASADENA CA 91109-8099
4	POULTER LAB D CURRAN R KLOOP L SEAMAN D SHOCKEY SRI INTERNATIONAL 333 RAVENSWWOD AVE MENLO PARK CA 94025

NO. OF COPIES	ORGANIZATION
1	UNIV OF DAYTON R HOFFMAN 300 COLLEGE PARK DAYTON OH 45469
6	INST FOR ADV TECH UNIV OF TX AT AUSTIN H FAIR S BLESS D LITTLEFIELD M NORMANDIA R SUBRANMANIAN T KIEHNE 4030 2 W BRAKER LN AUSTIN TX 78759
3	UNIV OF DAYTON RSRCH INST N BRAR A PIEKUTOWSKI D GROVE KLA14 300 COLLEGE PARK DAYTON OH 45469-0182
2	THE PENN STATE UNIV COLLEGE OF ENGR DR T KRAUTHAMMER DR R QUNEEY UNIV PARK PA 16802
2	SOUTHWEST RSRCH INST C ANDERSON J RIEGEL 6220 CULEBRA RD SOUTHWEST SAN ANTONIO TX 78238
2	UNIV OF CA SAN DIEGO S NEMAT NASSER M MEYERS DEPT OF APPLIED MECHS & ENGR SVCS RO11 LA JOLLA CA 92093-0411
2	CA RSCH & TECH CORP ROBERT BROWN DENNIS ORPHAL 5117 JOHNSON DR PLEASONTON CA 94566

NO. OF COPIES	ORGANIZATION
2	BROWN UNIV M CLIFTON S SUNDARAM DIV OF ENGR PROVIDENCE RI 02912
1	ROCKWELL INTL ROCKETDYNE DIV J MOLDENHAUER 6633 CANOGA AVE HB 23 CANOGA PK CA 91303
2	ALLIED SIGNAL L LIN PO BOX 31 PETERSBURG VA 23804
1	MCDONNELL DOUGLAS HELICOPTER L R BIRD MS 543 D216 5000 E MCDOWELL RD MESA AZ 85205
1	AEROJET PRECISION WPNS DEPT 5131 T W JOSEPH CARLEONE 1100 HOLLYVALE AZUSA CA 91702
1	PHYSICS INTL JIM COFFENBERRY 2700 MERCED ST PO BOX 5010 SAN LEANDRO CA 94577
1	BOEING CORP T M MURRAY MS 84 84 PO BOX 3999 SEATTLE WA 98124
1	NUCLEAR METALS INC R QUINN 2229 MAIN ST CONCORD MA 01742

NO. OF COPIES	ORGANIZATION
3	DYNA EAST CORP P C CHOU R CICCARELLI W FLIS 3201 ARCH ST PHILADELPHIA PA 19104
2	ALLIANT TECHSYSTEMS INC G R JOHNSON C CANDLAND MN 48 2700 7225 NORTHLAND DR BROOKLYN MN 55428
2	GENERAL RSCH CORP ALEX CHARTERS TOM MENNA PO BOX 6770 SANTA BARBARA CA 93160-6770
1	S CUBED R SEDGWICK PO BOX 1620 LA JOLLA CA 92038-1620
2	ORLANDO TECH INC D MATUSKA J OSBORN PO BOX 855 SHALIMAR FL 32579
1	KAMAN SCIENCES CORP D BARNETTE PO BOX 7463 CO SPRINGS CO 80933-7463
1	LIVERMORE SOFTWARE TECH CORP JOHN O HALLQUIST 2876 WAVERLY WAY LIVERMORE CA 94550
2	MARTIN MARIETTA MISSILE SYSTEMS C E HAMMOND MP 004 L WILLIAMS MP 126 PO BOX 555837 ORLANDO FL 32855-5837

NO. OF COPIES	ORGANIZATION
1	BATTELLE DALE TROTT 505 KING AVE COLUMBUS OH 43201
1	ZERNOW TECH SVCS INC LOUIS ZERNOW 425 W BONITA AVE SUITE 208 SAN DIMAS CA 91773
1	OLIN FLINCHBAUGH DIV RALF CAMPOLI 200 E HIGH ST PO BOX 127 RED LION PA 17356
2	E I DUPONT CO OSWALD BERGMANN BRIAN SCOTT BRANDYWINE BLDG RM 12204 WILMINGTON DE 19898
3	SIMULA INC R HUYETT G GRACE G YANIV 10016 S 51ST ST PHOENIX AZ 85044
1	LANXIDE CORP 1300 MARROWS RD PO BOX 6077 NEWARK DE 19714
1	BRIGGS CO J BACKOFEN 2668 PETERBOROUGH ST HERNDON VA 22071
1	SCHWARZKOPFF TECH CORP E KOSINISKI 35 JEFFREY AVE HOLLISTON MA 01746
1	PRIMEX CORP. D EDMONDS 10101 9TH ST N ST PETERSBURG FL 33716

NO. OF COPIES	ORGANIZATION
1	BATTELLE DR D TROTT 505 KING AVE COLUMBUS OH 43201
1	RAYTHEON CO R LLOYD PO BOX 1201 TEWKSBURY MA 01876
1	COORS CERAMICS CO MR R PARICIO STRUCTURAL DIV 600 NINTH ST GOLDEN CO 80401
1	INGALLS SHIPBUILDING CBI 01 MR P GREGORY PO BOX 149 PASCAGOULA MS 39567
4	UNITED DEFENSE LP V HORVATICH R RAJAGOPAL M MIDDIONE J MARROW PO BOX 359 SANTA CLARA CA 95052-0359
1	ALME AND ASSOC M ALME 9650 SANTIAGE RD STE 102 COLUMBIA MD 21045
3	LANXIDE ARMOR PRODUCTS K LEIGHTON V KELSEY R WOLFE 1300 MARROWS RD NEWARK DE 19714-6077
2	AERONAUTICAL RSRCH ASSOC R CONTILLIANO J WALKER 50 WASHINGTON RD PRINCETON NJ 08540

NO. OF COPIES	ORGANIZATION
1	THE CARBORUNDUM CO R PALIA PO BOX 1054 NIAGRA FALLS NY 19302
3	CERCOM INC R PALICKA A EZIS G NELSON 1960 WATSON WAY VISTA CA 92083
1	CENTURY DYNAMICS INC N BIRNBAUM 7700 EDGEWATER DR SUITE 626 OAKLAND CA 94621
1	APPLIED RSRCH ASSOCS INC J YATTEAU 5941 SO MIDDLEFIELD RD SUITE 100 LITTLETON CO 801123
1	ADELMAN ASSOC C CLINE 3301 EL AMINO RIAL SUITE 280 ATHERTA CA 94027
1	CYPRESS INTERNATIONAL A CAPONECCHI 1201 E ABINGDON DR ALEXANDRIA VA 22314
1	DOW CHEMICAL INC K EPSTEIN ORDNANCE SYS 800 BUILDING MIDLAND MI 48667
1	CALKINS R&D INC N CALKINS 515 SEWARD PK AVE ALBUQUERQUE NM 87123
1	KERAMONT CORPORATION E SAVRUN 4231 S FREEMONT AVE TUCSON AZ 85714

NO. OF COPIES	ORGANIZATION
1	SAIC J FURLONG MS 264 1710 GOODRIDGE DR PO BOX 1303 MCLEAN VA 22102
2	ALLIANT TECHSYSTEMS INC T HOLMQUIST G JOHNSON 7225 NORTHLAND DR BROOKLYN PARK MN 55428
2	GDLS W BURKE J ERIDON PO BOX 2094 WARREN MI 48090
1	BATTELLE EDGEWOOD A RICCHIAZZI 2113 EMMORTON PARK RD EDGEWOOD MD 21040
1	CORNING INC S HAGG SP DV 22 CORNING NY 14831
1	COORS CERAMICS CO STRUCTURAL DIV 600 NINTH ST GOLDEN CO 80401
1	O GARA HESS & EISENHARDT C WILLIAMS 9113 LE SAINT DR FAIRFIELD OH 45014
1	R J EICHELBERGER 409 W CATHERINE ST BEL AIR MD 21014-3613

NO. OF COPIES	ORGANIZATION
	ABERDEEN PROVING GROUND
63	DIR USARL AMSRL WM MF D DANDEKAR S CHOU (16 CPS) AMSRL WM TA W GILLICH T HAVEL W BRUCHEY S BILYK M BURKINS J DEHN M DUFFY G FILBEY W GOOCH D HACKBARTH G HAUVER E HORWATH G BULMASH Y HUANG M KEELE H MEYER E RAPACKI W ROWE J RUNYEON N RUPERT (10 CPS) M ZOLTOSKI AMSRL WM TB T WRIGHT AMSRL WM TC L MAGNESS W DE ROSSET W WALTERS M LAMPSON E KENNEDY K KIMSEY F GRACE (6 CPS) AMSRL WM TD D DIETRICH K FRANK S SEGLETES

NO. OF COPIES	ORGANIZATION
3	FRANHOFER INSTITUT FÜR KURZZEITDYNAMIK ERNST MACH INSTITUT H SENF E STRAßBURGER H ROTENHÄUSLER HAUPTSTRASSE 18 D 79 576 WEIL AM RHEIN GERMANY
3	FRANHOFER INSTITUT FÜR KURZZEITDYNAMIK ERNST MACH INSTITUT THOMA A STILP V HOHLER ECKERSTRAßE 4 D 79 104 FREIBURG GERMANY
3	DEUTSCH FRANZÖSISCHES FORSCHUNGSINSTITUT SAINT LOUIS H ERNST H LERR K HOOG CÉDEX 5 RUE DU GÉNÉRAL CASSAGNOU F 68301 SAINT LOUIS FRANCE
5	DEFENCE RSRCH AGENCY W CARSON T HAWKINS B SHRUBSALL C FREW I CROUCH CHOBHAM LANE CHERTEY SURRETY KT16 OEE UNITED KINGDOM
1	DEFENCE RSRCH AGENCY T BARTON FT HALSTEAD SEVEN OAKS KENT TN14 7BP UNITED KINGDOM
1	BATTELLE INGENIEURTECHNIK GMBH W FUCHE DUESSELDORFLER STR 9 D 65760 ESCHBORN GERMANY
1	DEUTSCHE AEROSPACE AG M HELD POSTFACH 12 40 D 86 523 SCHROBENHAUSEN GERMANY
5	RAPHAEL BALLISTICS CENTER Y PARTOM G ROSENBERG M MAYSELESS Z ROSENBERG Y YESHURUN BOX 2250 HAIFA 31021 ISRAEL
1	DYNAMEC RSRCH AB Å PERSSON PARADISGRÄND 7 S 151 36 SÖDERTÄLJE SWEDEN
1	DEFENCE RESEARCH ESTABLISHMENT SUFFIELD C WEICKERT BOX 4000 MEDICINE HAT ALBERTA TIA 8K6 CANADA
4	CENTRE DE RECHERCHES ET D'ETUDES D'ARCUEIL F TARDIVAL C COTTENNOT S JONNEAUX H ORSINI 16 BIS AVENUE PRIEUR DE LA CÔTE D'OR F 94114 ARCUEIL CÉDEX FRANCE

NO. OF COPIES	ORGANIZATION
1	INGENIEURBÜRO DEISENROTH F DEISENROTH AUF DE HARDT 33 35 D 5204 LOHMAR 1 GERMANY
1	CONDAT K THOMA MAXILLANSTR 28 8069 SCHEYERN FERNHAG GERMANY
1	EMBASSY OF AUSTRALIA DR R L WOODWARD 1601 MASS AVE NW WASHINGTON DC 20036-2273
3	SWEDISH DEFENCE RSRCH ESTABLISHMENT B JANZON I MELLGARD L HOLMBERG BOX 551 S 147 25 TUMBA SWEDEN
2	TNO PRINS MAURITS LAB H PASMAN R YSSELSTEIN PO BOX 45 2280 AA RIJSWIJK LANGE KLEIWEG 137 RUSWIJK NETHERLANDS
2	DEFENCE TECHNOLOGY AND PROCUREMENT AGENCY G LAUBE W ODERMATT BALLISTICS WEAPONS AND COMBAT VEHICLE TEST CENTER CH 3602 THUN SWITZERLAND
1	CELSIUS MATERIAL TEKNIK KARLSKOGA AB L HELLNER S 691 80 KARLSKOGA SWEDEN

NO. OF COPIES	ORGANIZATION
1	SWISS FEDERAL ARMAMENT WORKS W LANZ ALLMENDSSTRASSE 86 CH 3602 THUN SWITZERLAND
1	HIGH ENERGY DENSITY RSRCH CENTER G KANEL V FORTOV IZHORSKAYA 13 19 MOSCOW 127412 RUSSIAN REPUBLIC
1	IOFFE PHYSICO TECHNICAL INSTITUTE A KOZHUSHKO ST PERTERBURG 194021 RUSSIAN REPUBLIC
4	AERNAUTICAL & MARITIME RESEARCH LAB N BURMAN S CIMPOERU G WESTON E GELLERT PO BOX 4331 MELBOURNE VIC 3001 AUSTRALIA
1	TECHNION INSTITUTE OF TECHNOLOGY FACULTY OF MECHANICAL ENG. S BODNER TECHNION CITY HAIFA 32000 ISRAEL
2	FEDERAL MINISTRY OF DEFENCE DIRECTORATE FOR EQUIPMENT & TECHLAND RÜ V 2 D HAUG L REPPER POSTFACH 1328 53003 BONN GERMANY
1	CENTER d'ETUDES GRAMAT J CAGNOUX 46500 GRAMAT FRANCE

REPORT DOCUMENTATION PAGE

Form Approved
OMB No. 0704-0188

1. AGENCY USE ONLY *(Leave blank)*	2. REPORT DATE	3. REPORT TYPE AND DATES COVERED
	August 1997	Final, Jan 96-Sep 96

4. TITLE AND SUBTITLE
Energy Partitioning and Microstructural Observations Related to Perforation of Titanium and Steel Targets

5. FUNDING NUMBERS
AH80 TEDD01 68T8Gd
AH80 TEDD01 68T8X6

6. AUTHOR(S)

N. L. Rupert, F. I. Grace, W. Huang,* L. E. Murr,* and C-S. Niou*

7. PERFORMING ORGANIZATION NAME(S) AND ADDRESS(ES)

U.S. Army Research Laboratory
ATTN: AMSRL-WM-TA
Aberdeen Proving Ground, MD 21005-5066

8. PERFORMING ORGANIZATION REPORT NUMBER

ARL-TR-1453

9. SPONSORING/MONITORING AGENCY NAMES(S) AND ADDRESS(ES)

10.SPONSORING/MONITORING AGENCY REPORT NUMBER

11. SUPPLEMENTARY NOTES

*Their address is: The University of Texas at El Paso, El Paso, TX 79968-0520.

12a. DISTRIBUTION/AVAILABILITY STATEMENT

Approved for public release; distribution is unlimited.

12b. DISTRIBUTION CODE

13. ABSTRACT *(Maximum 200 words)*

This report presents an analysis of two target materials and the associated energetics related to the initial penetration into the target and perforation as the penetrator exits the target. Impact tests were conducted for tungsten alloy (WA) rods, striking rolled homogeneous armor (RHA), and titanium alloy plates. Rod-impact velocities were nominal 1,500 and 2,000 m/s. Target thicknesses were chosen so that the rods would overmatch the targets and lose some 200 m/s during penetration. The tests utilized flash x-rays to determine rod residual lengths and velocities and target plug features, to include thicknesses and velocities. From these observables, experimental determination of the corresponding kinetic energies (KEs) and estimates for the fracture energies were obtained. Also, in each case, target material adjacent to penetration-channel walls was examined by optical and electron microscopy and x-ray diffraction to gain further insight into deformation processes (cavity expansion) during penetration. The analytic penetration model gave results that were in good agreement with the experimental observables. In addition, it was observed that the RHA follows traditional plastic flow of cavity expansion, while WA shows deformation features that deviate significantly. The report discusses possible causes for these differences.

14. SUBJECT TERMS
titanium, steel, Grace-Tate Penetration Theory, microstructural analysis, kinetic energy, ordnance velocity, hypervelocity

15. NUMBER OF PAGES
37

16. PRICE CODE

17. SECURITY CLASSIFICATION OF REPORT	18. SECURITY CLASSIFICATION OF THIS PAGE	19. SECURITY CLASSIFICATION OF ABSTRACT	20. LIMITATION OF ABSTRACT
UNCLASSIFIED	UNCLASSIFIED	UNCLASSIFIED	UL

NSN 7540-01-280-5500
Standard Form 298 (Rev. 2-89)
Prescribed by ANSI Std. 239-18 298-102

INTENTIONALLY LEFT BLANK.

USER EVALUATION SHEET/CHANGE OF ADDRESS

This Laboratory undertakes a continuing effort to improve the quality of the reports it publishes. Your comments/answers to the items/questions below will aid us in our efforts.

1. ARL Report Number/Author ARL-TR-1453 (Rupert) Date of Report August 1997

2. Date Report Received _____

3. Does this report satisfy a need? (Comment on purpose, related project, or other area of interest for which the report will be used.) _____

4. Specifically, how is the report being used? (Information source, design data, procedure, source of ideas, etc.) _____

5. Has the information in this report led to any quantitative savings as far as man-hours or dollars saved, operating costs avoided, or efficiencies achieved, etc? If so, please elaborate. _____

6. General Comments. What do you think should be changed to improve future reports? (Indicate changes to organization, technical content, format, etc.) _____

CURRENT ADDRESS

_____
Organization

_____
Name E-mail Name

_____
Street or P.O. Box No.

_____
City, State, Zip Code

7. If indicating a Change of Address or Address Correction, please provide the Current or Correct address above and the Old or Incorrect address below.

OLD ADDRESS

_____
Organization

_____
Name

_____
Street or P.O. Box No.

_____
City, State, Zip Code

(Remove this sheet, fold as indicated, tape closed, and mail.)

(DO NOT STAPLE)

DEPARTMENT OF THE ARMY

OFFICIAL BUSINESS

NO POSTAGE
NECESSARY
IF MAILED
IN THE
UNITED STATES

BUSINESS REPLY MAIL
FIRST CLASS PERMIT NO 0001,APG,MD

POSTAGE WILL BE PAID BY ADDRESSEE

DIRECTOR
US ARMY RESEARCH LABORATORY
ATTN AMSRL WM TA
ABERDEEN PROVING GROUND MD 21005-5066